High-precision tracking of sperm swimming fine structure provides strong test of resistive force theory

B. M. Friedrich[1],*, I. H. Riedel-Kruse[2],†, J. Howard[2],‡ and F. Jülicher[1],§

[1]Max Planck Institute for the Physics of Complex Systems, Dresden, Germany and [2]Max Planck Institute for Molecular Cell Biology and Genetics, Dresden, Germany

*Present address: Department of Materials and Interfaces, Weizmann Institute of Science, Rehovot, Israel
†Present address: Department of Bioengineering, Stanford University, Stanford, CA, USA
‡howard@mpi-cbg.de
§Author for correspondence (julicher@pks.mpg.de)

SUMMARY

The shape of the flagellar beat determines the path along which a sperm cell swims. If the flagellum bends periodically about a curved mean shape then the sperm will follow a path with non-zero curvature. To test a simple hydrodynamic theory of flagellar propulsion known as resistive force theory, we conducted high-precision measurements of the head and flagellum motions during circular swimming of bull spermatozoa near a surface. We found that the fine structure of sperm swimming represented by the rapid wiggling of the sperm head around an averaged path is, to high accuracy, accounted for by resistive force theory and results from balancing forces and torques generated by the beating flagellum. We determined the anisotropy ratio between the normal and tangential hydrodynamic friction coefficients of the flagellum to be 1.81±0.07 (mean±s.d.). On time scales longer than the flagellar beat cycle, sperm cells followed circular paths of non-zero curvature. Our data show that path curvature is approximately equal to twice the average curvature of the flagellum, consistent with quantitative predictions of resistive force theory. Hence, this theory accurately predicts the complex trajectories of sperm cells from the detailed shape of their flagellar beat across different time scales.

Supplementary material available online at http://jeb.biologists.org/cgi/content/full/213/8/1226/DC1

Key words: sperm cell, flagellar propulsion, flagellar beat pattern, curvature.

INTRODUCTION

Sperm cells are propelled in a liquid by regular bending waves of a whip-like cell appendage called the flagellum (Gray, 1955). Flagellar propulsion results in complex trajectories of sperm cells. On short time scales, the sperm head undergoes a wiggling motion with the same frequency as the flagellar beat. This wiggling of the sperm head is a consequence of balancing the forces and torques generated by the beating flagellum and characterizes the 'fine structure' of sperm swimming. On a time scale longer than the period of the flagellar beat, sperm cells of many species swim along circular or helical paths (Rikmenspoel et al., 1960; Goldstein, 1977; Brokaw, 1979; Crenshaw, 1996; Corkidi et al., 2008). The non-zero curvature of their paths is a consequence of asymmetric flagellar waves, and plays a vital role in sperm chemotaxis (Miller, 1985; Kaupp et al., 2008; Friedrich and Jülicher, 2007).

How the observed complex swimming paths of sperm cells and other microswimmers emerge from their swimming strokes is an important question of long-standing interest (Gray and Hancock, 1955; Rikmenspoel, 1965; Brokaw, 1970; Yundt et al., 1975; Smith et al., 2009). In pioneering work, Taylor demonstrated that self-propulsion is possible due to purely viscous forces (Taylor, 1951). Gray and Hancock introduced a local hydrodynamic theory of flagellar propulsion that neglects long-range hydrodynamic interactions and focuses on anisotropic local hydrodynamic friction between the sperm surface and the adjacent fluid (Gray and Hancock, 1955). This theory is commonly known as resistive force theory. The net swimming speed predicted by this theory depends

strongly on the anisotropy ratio of flagellar friction coefficients. The precise value of this key parameter has been subject to debate (Gray and Hancock, 1955; Brokaw, 1970; Cox, 1970; Shack et al., 1974; Lighthill, 1976; Brennen and Winet, 1977; Johnson and Brokaw, 1979). The theory of Gray and Hannock was later refined by Lighthill using slender-body approximations for the thin flagellum to include long-range hydrodynamic interactions (Lighthill, 1976). Other groups proposed even more advanced hydrodynamic simulation schemes (Dresdner and Katz, 1981; Elgeti and Gompper, 2008; Smith et al., 2009). For swimming in the vicinity of a solid surface, resistive force theory provides a simple and concise theoretical approach to flagellar propulsion. It has been used in several studies to account for experimental data (Gray and Hancock, 1955; Rikmenspoel et al., 1960; Brokaw, 1970; Yundt et al., 1975; Keller and Rubinow, 1976).

In the present work, we used theory and experiment to address how the swimming path of a sperm cell is determined by the shape of its flagellar bending waves. To test the resistive force theory of flagellar propulsion, we accurately measured the fine structure of the oscillatory movements of the sperm head. This approach is novel and depends crucially on the precision of the tracking data [see Yundt et al. for an early attempt (Yundt et al., 1975)]. To facilitate sperm tracking, we made use of the fact that sperm cells become hydrodynamically trapped near a planar boundary surface (Woolley, 2003): there they swim in a plane parallel to the surface with an approximately planar flagellar beat, allowing one to confine the analysis to two spatial dimensions. Using

tracked flagellar beat patterns, we could accurately reconstruct instantaneous velocities of sperm swimming using resistive force theory. From our analysis, we determined the drag anisotropy ratio.

On time scales longer than the period of the flagellar beat, sperm trajectories near a boundary surface are circular (Rikmenspoel et al., 1960; Goldstein, 1977; Brokaw, 1979; Woolley, 2003; Kaupp et al., 2008; Riedel-Kruse et al., 2007). The non-zero curvature of these swimming paths was shown to correlate with an asymmetry of the flagellar beat pattern in its plane of beating (Rikmenspoel et al., 1960; Goldstein, 1977; Brokaw, 1979). We re-investigated the relationship between mean flagellar curvature (characterizing flagellar beat asymmetry) and the resulting curvature of the sperm swimming path and found a linear dependence between the two curvatures, with a factor of proportionality significantly larger than one. We demonstrate that this counter-intuitive result is due to the non-linear nature of flagellar propulsion and can be understood in the framework of resistive force theory as a result of the finite amplitude of the flagellar bending waves and the hydrodynamic friction of the sperm head.

MATERIALS AND METHODS
Tangent angle representation of planar flagellar beat patterns
For sperm cells swimming close to a planar boundary surface, almost planar beat patterns were observed with a plane of flagellar beating approximately parallel to the boundary surface. In our analysis, we neglected any out-of-plane component of the flagellar beat, and considered the two-dimensional projection of the flagellar shape on the plane of swimming. We describe the (projected) shape of the bent flagellum at a given time t by the position vector $\mathbf{r}(s,t)$ of points along the centreline of the flagellum, where s is the arc length along the centreline (Fig. 1). We express $\mathbf{r}(s,t)$ with respect to the material frame of the sperm head: let $\mathbf{r}(t)$ be the position vector of the centre of the sperm head and $\mathbf{e}_1(t)$ a unit vector parallel to the long axis of the sperm head. Additionally, we define a second unit vector $\mathbf{e}_2(t)$, which is obtained by rotating $\mathbf{e}_1$ in the swimming plane by an angle of $\pi/2$ in a counter-clockwise fashion. With this notation, $\mathbf{r}+r_1\mathbf{e}_1$ corresponds to the proximal tip of the sperm head while $\mathbf{r}-r_1\mathbf{e}_1$ corresponds to the proximal end of the flagellum; here $2r_1\approx10\,\mu m$ is the length of the head along its long axis $\mathbf{e}_1$. The shape of the flagellar centreline $\mathbf{r}(s,t)$ at time t is characterized by a tangent angle $\psi(s,t)$ for each arc length position s, $0\leq s\leq L$, where L is the length of the flagellum. The tangent angle measures the angle enclosed by the vector $\mathbf{e}_1(t)$ and the tangent vector to the flagellar centreline at $\mathbf{r}(s,t)$ (see Fig. 1). Note that the derivative of $\psi(s,t)$ with respect to arc length s is the local curvature of the flagellar centreline. For a regular flagellar beat pattern, the tangent angle $\psi(s,t)$ is a periodic function of t with period $T=2\pi/\omega$, where ω is the angular frequency of the flagellar beat. From the tangent angle $\psi(s,t)$, the position $\mathbf{r}(t)$ of the sperm head and its material frame defined by $\mathbf{e}_1(t)$ and $\mathbf{e}_2(t)$, we can reconstruct the full flagellar beat pattern as:

$$\mathbf{r}(s,t) = \mathbf{r}(t) - r_1\mathbf{e}_1(t) - \int_0^s du \cos\psi(u,t)\mathbf{e}_1(t) + \sin\psi(u,t)\mathbf{e}_2(t) . \quad (1)$$

In our experiments with bull sperm, the tangent angle of the flagellar wave was well described by its zeroth and the first Fourier mode (Riedel-Kruse et al., 2007):

$$\psi(s,t) \approx \tilde{\psi}_0(s) + \tilde{\psi}_1(s)e^{i\omega t} + \tilde{\psi}_1^*(s)e^{-i\omega t}, \quad (2)$$

where $\tilde{\psi}_1^*$ denotes the complex conjugate of $\tilde{\psi}_1$. Higher modes contribute less than 5% to the power spectrum of the tangent angle at all arc-length positions s. The zeroth mode $\tilde{\psi}_0$ characterizes a

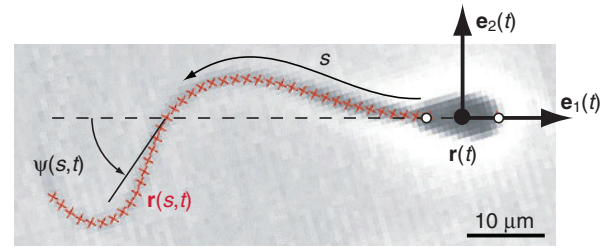
Fig. 1. Snapshot of a beating bull sperm (at a time t). We chose a material frame for the sperm head with orthonormal vectors $\mathbf{e}_1(t)$ and $\mathbf{e}_2(t)$ such that $\mathbf{e}_1(t)$ is parallel to the long axis of the head. The shape of the flagellum is characterized by the tangent angle $\psi(s,t)$ as a function of arc length s: $\psi(s,t)$ is the angle enclosed by the long axis of the sperm head and the local tangent of the flagellar centreline at position $\mathbf{r}(s,t)$.

time-averaged mean shape of the flagellum; whereas, the amplitude of the first mode, $|\tilde{\psi}_1|$, gives the amplitude of the principal bending wave of the flagellum.

Fig. 2 shows the zeroth and first Fourier mode as a function of arc length s along the flagellum for two representative sperm cells (observed at different fluid viscosities). From the Fourier decomposition, we obtain three parameters that characterize key features of the shape of the flagellar beat. First, the mean flagellar curvature K_0 is defined by fitting a line $K_0 s$ to the zeroth mode $\tilde{\psi}_0(s)$; K_0 provides a simple measure for the asymmetry of the mean shape of the flagellum. Note that the ideal case $\tilde{\psi}_0(s)=K_0 s$ corresponds to a mean shape of the flagellum that is curved in a perfect arc with constant curvature K_0. Second, the amplitude parameter A_0 is defined by fitting the line $A_0 s$ to the absolute value of the first mode $|\tilde{\psi}_1(s)|$. The ideal case $|\tilde{\psi}_1|=A_0 s$ corresponds to a bending amplitude that increases linearly along the flagellum. Third, the wavelength λ of the principal flagellar bending wave is defined by fitting the line $2\pi s/\lambda$ to the phase angle $\varphi(s)=-\arg\tilde{\psi}_1(s)$ of the (complex) first Fourier mode. The ideal case $\varphi(s)=2\pi s/\lambda$ corresponds to a travelling wave with uniform wavelength λ and wave speed $\lambda\omega/(2\pi)$.

Instantaneous *versus* effective swimming speeds
Instantaneous velocities
For planar swimming, the head of a sperm cell can move parallel and perpendicular to its long axis, as well as rotate around an axis normal to the plane of swimming. Thus, planar sperm swimming is characterized by three degrees of freedom. We characterize the translational motion of the sperm head with respect to the head's material frame introduced in Fig. 1 by time-dependent velocity components $v_1(t)$ and $v_2(t)$ such that:

$$\dot{\mathbf{r}}(t) = v_1(t)\mathbf{e}_1(t) + v_2(t)\mathbf{e}_2(t) . \quad (3)$$

Here dots denote time derivatives. Rotation of the sperm head is characterized by an instantaneous angular speed $\Omega(t)$ such that:

$$\dot{\mathbf{e}}_1(t) = \Omega(t)\mathbf{e}_2(t) ,$$
$$\dot{\mathbf{e}}_2(t) = -\Omega(t)\mathbf{e}_1(t) . \quad (4)$$

Effective net speeds
In experiments with bull sperm cells, the centre of the sperm head moved along a complex trajectory $\mathbf{r}(t)$ that wiggled around an averaged path $\bar{\mathbf{r}}(t)$ (Gray, 1955; Rikmenspoel, 1965) (Fig. 3). The averaged path $\bar{\mathbf{r}}(t)$ describes the effective net motion of the whole
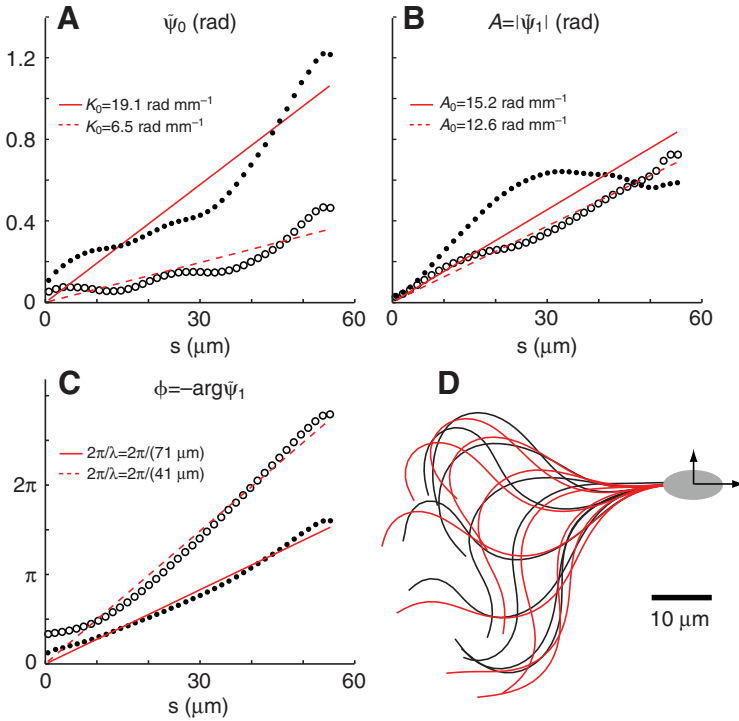
Fig. 2. Fourier representation of the flagellar beat of a swimming bull sperm cell. (A–C) Different Fourier modes of the tangent angle $\psi(s)$ for the case of normal viscosity $\eta=0.7\,\text{mPa s}$ (solid circles) or increased viscosity $\eta=10\,\text{mPa s}$ (open circles): panel A shows the zeroth Fourier mode $\tilde{\psi}_0(s)$ which characterizes the asymmetry of the mean shape of the flagellum; panel B shows the absolute value $|\tilde{\psi}_1(s)|$ of the first Fourier mode which characterizes the amplitude of the principal flagellar bending wave; and finally panel C shows the phase angle $\phi(s)=-\text{arg}\tilde{\psi}_1(s)$ of the first Fourier mode which characterizes the wave speed of the principal flagellar wave. By fitting straight lines to these experimental data, we derive three parameters which characterize the shape of the flagellar beat; these parameters are mean flagellar curvature K_0 (A), the amplitude rise A_0 of the principal flagellar wave (B), and the wavelength λ of this wave (C). The linear fits are shown as solid and dashed red lines for the case of normal and increased viscosity, respectively. (D) Shown in red are flagellar shapes reconstructed from the zeroth and first Fourier component of the tangent angle $\psi(s,t)$ for the case of normal viscosity at subsequent times 4 ms apart. For comparison, the experimentally observed flagellar shape is shown in black for eight subsequent frames (also 4 ms apart).

sperm cell on a coarse-grained time scale, which averages over several beat cycles. This effective motion is characterized by effective translational and rotational speeds, $\bar{v}=\Delta s/\Delta t$ and $\bar{\Omega}=\Delta\Phi/\Delta t$, respectively. Here the time interval $\Delta t=nT$ comprises several beat cycles, whereas Δs measures the distance travelled along the path $\bar{\mathbf{r}}$ and $\Delta\Phi$ is the net rotation of the sperm head. It should be emphasized that $\bar{v}$ is not simply the time average of the instantaneous parallel velocity $v_1(t)$, but has to be determined from the averaged swimming path $\bar{\mathbf{r}}(t)$. The curvature of the averaged path $\bar{\mathbf{r}}$ is given by $\kappa=1/r_0=\bar{\Omega}/\bar{v}$ where r_0 is the radius of the circular path $\bar{\mathbf{r}}$. In the literature, $v=|\dot{\mathbf{r}}|$ is sometimes referred to as curvilinear velocity (VCL) and $\bar{v}=|\dot{\bar{\mathbf{r}}}|$ as velocity along the averaged path (VAP).

Reconstructing instantaneous velocities from flagellar beat patterns

The swimming of sperm cells is characterized by low Reynolds numbers implying that inertial forces are negligible (Purcell, 1977; Landau and Lifshitz, 1987). We compute instantaneous swimming velocities from recorded flagellar beat patterns in the limit of zero Reynolds number using the resistive force theory introduced by Gray and Hancock (Gray and Hancock, 1955). This local hydrodynamic theory neglects long-range hydrodynamic interactions and assumes that the hydrodynamic drag force density $\mathbf{f}(s)$ that acts on a cylindrical portion of the filament at arc length s is linear in the local velocity components $\mathbf{v}_\parallel(s,t)=[\dot{\mathbf{r}}(s,t)\cdot\mathbf{t}(s,t)]\mathbf{t}(s,t)$ and $\mathbf{v}_\perp(s,t)=\dot{\mathbf{r}}(s,t)-\mathbf{v}_\parallel(s,t)$ parallel and perpendicular to the filament centreline, respectively:

$$\mathbf{f}(s,t) = \xi_\perp\mathbf{v}_\perp(s,t) + \xi_\parallel\mathbf{v}_\parallel(s,t) . \quad (5)$$

Here the dot denotes differentiation with respect to time t and $\mathbf{t}(s,t)$ is the tangent vector of the flagellar centreline at position $\mathbf{r}(s,t)$. Note that the proximal tip of the flagellum $\mathbf{r}(s=0,t)$ moves in synchrony with the head centre, i.e. $\mathbf{v}_\parallel(s=0,t)=v_1(t)\mathbf{e}_1(t)$ and $\mathbf{v}_\perp(s=0,t)=[v_2(t)+r_2\Omega(t)]\mathbf{e}_2(t)$, as the sperm head is assumed to be rigid. One can envisage the approach of resistive force theory by approximating the bent filament as a sequence of straight rods

connected at their ends and then computing the drag force density for the individual rods.

Force and torque balance

Since no external forces are acting on a freely swimming sperm cell (Gray and Hancock, 1955; Jülicher and Prost, 2009), the total hydrodynamic drag force $\mathbf{F}$ acting on the swimming sperm cell at time t must vanish:

$$\mathbf{F}(t) = \mathbf{F}_{\text{head}}(t) + \int_0^L \text{d}s\,\mathbf{f}(s,t) = 0 . \quad (6)$$
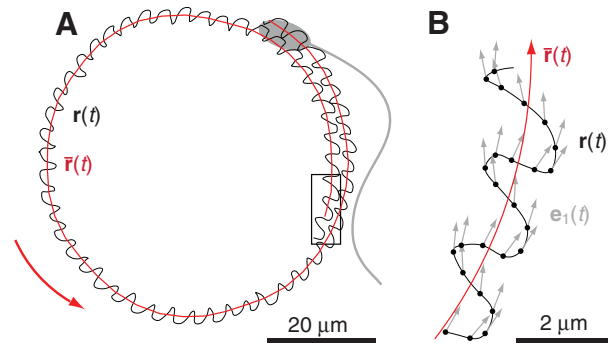

Fig. 3. Trajectory $\mathbf{r}(t)$ of the centre of the head of a swimming bull sperm cell (black) and averaged swimming path $\bar{\mathbf{r}}(t)$ (red); see also supplementary material Movie 1. (A) The motion of the head is the superposition of a uniform motion and a periodic movement with the frequency ω of the flagellar beat. Averaging over the period of the flagellar beat yields the averaged swimming path. In the present case, the averaged swimming path is a circular trajectory. For comparison, a schematic drawing of a sperm cell is shown to scale in grey. (B) Magnified view of the rectangular portion of panel A. Black dots indicate the measured positions of the sperm head; the black line interpolates between the data points. Grey arrows indicate the vector $\mathbf{e}_1$ parallel to the long axis of the head. The sampling rate was 250 frames s^{-1}.

Here $\mathbf{F}_{head}$ is the hydrodynamic drag force of the head. Similarly, the total torque $\mathbf{M}$ acting on the sperm cell must be zero as well:

$$\mathbf{M}(t) = \mathbf{M}_{head}(t) + \int_0^L ds\,\mathbf{f}(s,t) \times \mathbf{r}(s,t) = 0\,, \qquad (7)$$

where $\mathbf{M}_{head}$ is the hydrodynamic torque acting on the pivoting head. For planar swimming in a plane spanned by the vectors $\mathbf{e}_1(t)$ and $\mathbf{e}_2(t)$, we obtain three independent scalar equations $\mathbf{F}(t)\cdot\mathbf{e}_1(t)=0$, $\mathbf{F}(t)\cdot\mathbf{e}_2(t)=0$ and $\mathbf{M}(t)\cdot[\mathbf{e}_1(t)\times\mathbf{e}_2(t)]=0$. Using these three equations, we can compute the three instantaneous velocities $v_1(t)$, $v_2(t)$ and $\Omega(t)$ of the sperm head at any instant t in time provided the tangent angle $\psi(s,t)$ and its time derivative $\dot{\psi}(s,t)$ are known. These predicted velocities will then be compared with directly measured instantaneous velocities (Fig. 4).

Drag force of the head

To describe sperm swimming accurately, the hydrodynamic drag force $\mathbf{F}_{head}$ and the torque $\mathbf{M}_{head}$ of the moving head must be considered (Johnson and Brokaw, 1979). In our numeric calculations, we approximate the shape of the sperm head as a spheroid and use Perrin's formulas to express the hydrodynamic drag force and torque as $\mathbf{F}_{head}=\xi_1 v_1\mathbf{e}_1+\xi_2 v_2\mathbf{e}_2$ and $\mathbf{M}_{head}=\xi_{rot}\Omega\mathbf{e}_1\times\mathbf{e}_2$ (Perrin, 1934). We use $2r_1=10\,\mu m$ for the length of the head along the long axis $\mathbf{e}_1$ and $5\,\mu m$ for the length along the short axis $\mathbf{e}_2$ and obtain $\xi_1\approx40.3\,pN\,s\,mm^{-1}$, $\xi_2\approx46.1\,pN\,s\,mm^{-1}$ and $\xi_{rot}\approx0.84\,pN\,\mu m\,s$. These friction coefficients correspond to motion far from any boundary surface and thus only serve as a reference. For the case studied here, the proximity of the boundary surface is likely to increase the friction coefficients. Note that within the framework of resistive force theory only the ratios of friction coefficients play a role in determining swimming velocities.

High-speed videoscopy of swimming bull sperm

Sperm cells were obtained as frozen samples (IFN Schönow, Germany) and prepared as described previously (Riedel-Kruse et al., 2007). Swimming of sperm cells was studied in aqueous solution of viscosity $\eta\approx0.7\,mPa\,s$ at 36°C in a shallow observation chamber of 1 mm depth using phase-contrast microscopy (Axiovert 200M, Zeiss, Jena, Germany). Sperm swimming paths were recorded with a high-speed camera (FastCam, Photron, San Diego, CA, USA) at a rate of $250\,frames\,s^{-1}$ for a duration of 4 s in each case. Movies were analysed using custom-made Matlab routines (The MathWorks, Inc., Natick, MA, USA). For each frame, the position and orientation of the sperm head, as well as the tangent angle $\psi(s,t)$ at each tail point (relative to the orientation of the head) were computed. The precision of the automated tracking of the flagellum was of the order of 0.1 pixels, corresponding to 70 nm. The position of the elongated sperm head could be
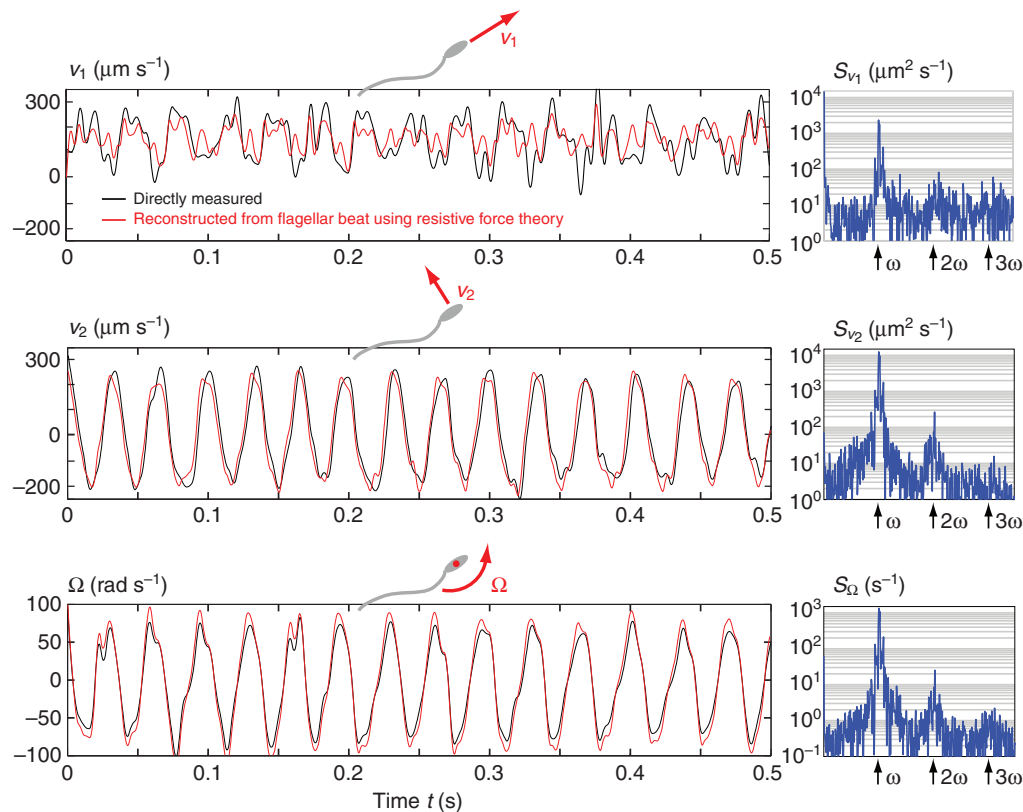

Fig. 4. Measured instantaneous velocities of the head of a bull sperm cell swimming in a plane close to a boundary surface (black). Planar motion of the rigid sperm head is characterized by three velocities: translational velocities v_1 and v_2 parallel and perpendicular to the long axis of the sperm head, and a rotational velocity Ω describing rotations in the plane of swimming. All swimming velocities oscillate with the frequency ω of the flagellar beat as reflected by corresponding power spectra S on the right (blue graphs). We used the recorded beat pattern to predict the swimming velocities using resistive force theory as specified in the main text ('Reconstructing instantaneous velocities from flagellar beat patterns') (red curves). We find good agreement between the time series of directly measured velocities and the corresponding time series of velocities reconstructed from the flagellar beat pattern. The tangential and normal friction coefficients $\xi_\perp$ and $\xi_\parallel$ used for reconstructing swimming velocities were obtained by a global fit (see 'Determining friction coefficients by comparing instantaneous velocities' above). The experimental errors in determining instantaneous velocities are of the order of $150\,\mu m\,s^{-1}$, $30\,\mu m\,s^{-1}$ and $15\,rad\,s^{-1}$ for v_1, v_2 and Ω, respectively.

Table 1. Experimentally determined friction coefficients and net swimming speeds

Sperm no.	$\xi_\parallel$ (fN s μm^{-2})	$\xi_\perp/\xi_\parallel$	$\bar{v}$ (μm s^{-1})	$\bar{\Omega}$ (rad s^{-1})	Experiment/theory	
					$\delta\bar{v}$	$\delta\bar{\Omega}$
1	1.93±0.08	1.79±0.04	149±3	1.9±0.4	5%	35%
2	0.45±0.06	1.76±0.04	124±8	3.4±0.3	3%	18%
3	0.36±0.03	1.79±0.03	97±3	3.3±0.4	5%	14%
(4)	(0.86±0.04)	(1.43±0.05)	(111±5)	(3.7±0.5)	(18%)	(24%)
5	0.38±0.04	1.89±0.02	105±8	4.1±0.4	6%	5%
6	0.31±0.04	1.87±0.04	94±8	3.3±0.5	3%	22%
7	0.73±0.14	1.72±0.06	141±11	2.2±0.3	8%	23%
ø	0.69±0.62	1.81±0.07	118±23	3.0±0.9	6%	19%

Time series of instantaneous velocity components recorded from seven different bull sperm cells were compared with corresponding time series reconstructed from the flagellar beat pattern tracked in the same experiment to determine the normal and parallel friction coefficients of the flagellum, $\xi_\perp$ and $\xi_\parallel$, respectively. Errors denote standard deviation (N=8, time series of duration 0.5 s per sperm cell). Additionally, we compared net speeds $\bar{v}$ and $\bar{\Omega}$ of progression along an averaged swimming path with corresponding values $\bar{v}_{theory}$ and $\bar{\Omega}_{theory}$ predicted from the flagellar beat pattern using the friction coefficients determined by the global fit. Displayed are the directly measured speeds $\bar{v}$ and $\bar{\Omega}$ as well as the root-mean-squared deviations $\delta\bar{v}$ and $\delta\bar{\Omega}$ between measured and reconstructed speeds with $\delta\bar{v}^2=\langle(\bar{v}_{theory}/\bar{v}-1)^2\rangle$. For $\delta\bar{\Omega}$, an analogous definition is used. When fitting the friction coefficients for sperm no. 4, the residual sum of squares was 50–100% larger than for the other cases; we therefore excluded sperm no. 4 in the further analysis. Data from sperm no. 5 were used to prepare Figs 2, 3 and 4 as well as supplementary material Movie 1.

determined in the direction parallel to its long axis with a precision of the order of 0.5 pixels, corresponding to 350 nm (Riedel-Kruse et al., 2007). In a final step of data processing, the tracking data for the individual frames were smoothly interpolated in time; see the black trajectory in Fig. 3B.

In a second series of experiments, we studied sperm swimming at an increased viscosity of $\eta \approx 10$ mPa s in an aqueous solution of Ficoll 400 (Sigma, #F-4375; St Louis, MO, USA). Viscosities were measured with a viscometer (Brookfield, Model DV-I +; Lorch, Germany) at a temperature of 36°C. Aqueous solutions of the highly branched polymer Ficoll 400 approximately behave as Newtonian fluids (Hunt et al., 1994).

Determining friction coefficients by comparing instantaneous velocities

Using high-precision tracking data for the position and orientation of the sperm head of swimming bull sperm cells, the instantaneous translational and rotational velocity components $v_1(t)$, $v_2(t)$ and $\Omega(t)$ as defined in Eqns 3 and 4 were measured. An example of the resulting time series of instantaneous velocities is shown in Fig. 4. In the same experiments, the flagellar beat pattern was recorded. We used these data to reconstruct the instantaneous velocities using a simple local hydrodynamics theory as specified above ('Reconstructing instantaneous velocities from flagellar beat patterns'). By a global least-squares fit of directly measured and reconstructed time series, we were able to determine the normal and the tangential friction coefficients of the flagellum, $\xi_\perp$ and $\xi_\parallel$, respectively. The results are summarized in Table 1; the means ± s.d. are $\xi_\parallel$=0.69±0.62 fN s μm^{-2} and $\xi_\perp/\xi_\parallel$=1.81±0.07.

Within the framework of resistive force theory, only the ratios of friction coefficients play a role in determining velocities. Therefore, the absolute values for $\xi_\parallel$ presented in Table 1 are determined relative to the friction coefficients ξ_1 and ξ_2 of the head only, estimated above ('Reconstructing instantaneous velocities from flagellar beat patterns'). The boundary surface increases the hydrodynamic friction of the sperm head, the increase being larger the closer the head is to the surface. Because we neglected the boundary in estimating the friction coefficients for the head, we are underestimating the friction coefficients of the flagellum. It has been reported that the distances between sperm cells swimming near a boundary surface and the surface itself are broadly distributed (with mean and standard deviation of the order of 10 μm) (Rothschild, 1963; Winet et al., 1984). Such a variable distance to the surface could account for the observed variability in the fit results for the coefficients of the flagellum.

Swimming at increased viscosity

In the case of high viscosity, $\eta \approx 10$ mPa s, we observed flagellar beat patterns that were different from the case of normal viscosity $\eta \approx 0.7$ mPa s studied above. Both the frequency of the flagellar beat and the wavelength of the flagellar bending waves were reduced, resulting in lower values for the net speed $\bar{v}$ of translational motion (see Table 2). Qualitatively similar results had been obtained earlier for invertebrate spermatozoa (Brokaw, 1966). Additionally, we report on the mean flagellar curvature K_0 as well as the net angular speed $\bar{\Omega}$ and find that these quantities are also reduced in the case of high viscosity.

Instantaneous velocities were reduced by a factor of about 10 in the case of high viscosity compared with the case of normal viscosity. This resulted in larger relative errors of the velocity data, and data quality was not sufficient to reliably compare time series of instantaneous velocities and determine friction coefficients. In the limit of zero Reynolds number, theory predicts that all friction coefficients scale linearly with viscosity.

Table 2. Flagellar beat patterns change with fluid viscosity

Viscosity η (mPa s)	T (ms)	K_0 (rad mm^{-1})	A_0 (rad mm^{-1})	λ (μm)	$\bar{v}$ (μm s^{-1})	$\bar{\Omega}$ (rad s^{-1})	N
0.7 (water at 36°C)	32±2	13.1±4.8	14.6±1.2	66±8	117±22	3.1±0.8	7
10	54±13	6.6±3.2	12.0±1.0	39±3	43±13	0.6±0.3	6

Displayed are parameters characterizing the flagellar beat pattern of bull sperm cells swimming close to a planar boundary surface for two values of fluid viscosity.

Discription of parameters: T, period of flagellar beat; A_0, amplitude rise of flagellar bending wave; λ, wavelength of flagellar bending wave; K_0, mean flagellar curvature; N, number of sperm cells analysed. Additionally, net speeds of translational and rotational motion, $\bar{v}$ and $\bar{\Omega}$, are shown.

RESULTS
Instantaneous swimming velocities oscillate with the frequency of the flagellar beat

Our tracking experiments with bull sperm cells swimming near a planar boundary surface reveal the fine structure of their swimming: the centre of the sperm head followed an intricate trajectory $\mathbf{r}(t)$ that wiggles around an averaged path $\bar{\mathbf{r}}(t)$ (see Fig. 3). With respect to its own material frame, the motion of the sperm head is characterized by three time-dependent velocities: translational velocities v_1 and v_2 parallel and perpendicular to the long axis of the sperm head, and a rotational velocity Ω describing rotations in the plane of swimming. Fig. 4 shows these (instantaneous) swimming velocities for the motion of the sperm head (black curves). All three swimming velocities oscillate with the frequency ω of the flagellar beat as is reflected by the corresponding power spectra on the right of Fig. 4 (blue graphs).

Theory predicts a fundamental difference between the velocity component v_1 and the other two components v_2 and Ω, as only the last two change their sign when the flagellar beat pattern is reflected along the long axis $\mathbf{e}_1$ of the sperm head. Based on this symmetry argument, we infer that in the limit of small tangent angles, v_1 should be a superposition of a non-zero average value and oscillatory modes with frequencies ω and 2ω (see Eqn A3 in the Appendix). Note that the occurrence of oscillations with twice the flagellar frequency is a result of the non-linear nature of flagellar propulsion and is not due to higher modes of the flagellar oscillations for the case considered here. We find confirmation of these theoretical predictions in our experimental data: in Fig. 4, v_1 indeed varies around a non-zero average value. Also, in the power spectrum S_{v1} of v_1, the power of the Fourier peak at frequency 2ω amounts to a considerable fraction $\rho_{v1} \approx 15\%$ of the power of the Fourier peak at frequency ω: oscillations with the beat frequency and twice the beat frequency superimpose. This feature was even more pronounced in the case of increased fluid viscosity with $\rho_{v1}=107\pm54\%$ (mean±s.d., $N=6$) compared with the case of normal viscosity with $\rho_{v1}=22\pm29\%$ ($N=7$). Analogously defined power ratios for the velocity components v_2 and Ω amount only to a few per cent.

Experimental determination of the drag anisotropy ratio

We used the recorded beat pattern to predict instantaneous swimming velocities using a simple local hydrodynamics theory (resistive force theory) as detailed above ('Reconstructing instantaneous velocities from flagellar beat patterns'). By adjusting the ratio between the normal and the tangential flagellar friction coefficient, $\xi_\perp$ and $\xi_\parallel$, we obtained good agreement between the predicted velocities and the measured ones (compare black and red curves in Fig. 4, and see Table 1). Remarkably, for 6 out of 7 sperm trajectories analysed, the drag anisotropy ratio $\xi_\perp/\xi_\parallel$ determined by the fit fell into a rather narrow range $\xi_\perp/\xi_\parallel \approx 1.81\pm0.07$ (mean±s.d., $N=6$).

The success of resistive force theory in predicting instantaneous swimming velocities is impressive, taking into account the fact that this theory neglects long-range hydrodynamic interactions between different parts of the moving flagellum. In our experiments, the long-range hydrodynamic interactions are partially screened by the proximity of the boundary surface of the observation chamber, which is much less than the wavelength of flagellar bending waves (Rothschild, 1963; Winet et al., 1984). Therefore, it is still possible that long-range hydrodynamic interactions play a significant role in determining sperm swimming paths in open water far from surfaces. Note also, that more sophisticated hydrodynamic theories are needed to explain why sperm cells become trapped near boundary surfaces in the first place (Elgeti and Gompper, 2008; Smith et al., 2009).

The precise value of the drag anisotropy ratio has been subject to debate (Gray and Hancock, 1955; Brokaw, 1970; Cox, 1970; Shack et al., 1974; Lighthill, 1976; Brennen and Winet, 1977; Johnson and Brokaw, 1979). In their original work, Gray and Hancock used the value $\xi_\perp/\xi_\parallel=2$, which is valid for a flagellum far from any boundary surface in the limit of a vanishing diameter of the flagellum. A drag anisotropy ratio of 2 also applies for a slender cylinder of finite thickness that moves parallel to a surface (Hunt et al., 1994). For flagella of finite thickness far from a surface, various approximations provided values of the drag anisotropy ratio in the range $\xi_\perp/\xi_\parallel=1.5$–1.8 (Cox, 1970; Shack et al., 1974; Lighthill, 1976; Brennen and Winet, 1977); when applied to the flagellar parameters of bull sperm cells, the most accurate approximations (Shack et al., 1974; Lighthill, 1976) give $\xi_\perp/\xi_\parallel=1.77$. An early attempt to experimentally determine the drag anisotropy ratio from the net angular speed $\bar{\Omega}$ for swimming near a boundary surface yielded $\xi_\perp/\xi_\parallel \approx 1.8$ (no error bars given) (Brokaw, 1970). Using a t-test, we calculate the 95% confidence interval from our six measurements of the anisotropy ratio to be [1.73,1.88]. Thus, our result is consistent with the earlier experimental value and also close to the value of 1.77 estimated previously for swimming far from surfaces.

How curved swimming paths arise from asymmetric beat patterns

The recorded flagellar beat pattern of bull sperm cells exhibits a pronounced asymmetry in the plane of beating, with a mean shape of the flagellum that has non-zero curvature (see Fig. 2A). To characterize flagellar asymmetry, we consider the mean flagellar curvature K_0, which is computed by fitting a line K_0s to the zeroth Fourier mode $\tilde{\psi}_0(0)$ of the tangent angle $\psi(s,t)$ (see 'Tangent angle representation of planar flagellar beat patterns' above).

As a consequence of the asymmetric flagellar beat, the resulting averaged swimming path $\bar{\mathbf{r}}$ is not straight, but has non-zero curvature κ. Fig. 5 displays experimental data correlating mean flagellar curvature K_0 and path curvature κ for 13 bull sperm cells swimming close to a boundary surface in normal and high viscosity solutions. We find that path curvature κ scales approximately linearly with mean flagellar curvature K_0, with a proportionality factor of 2.2.
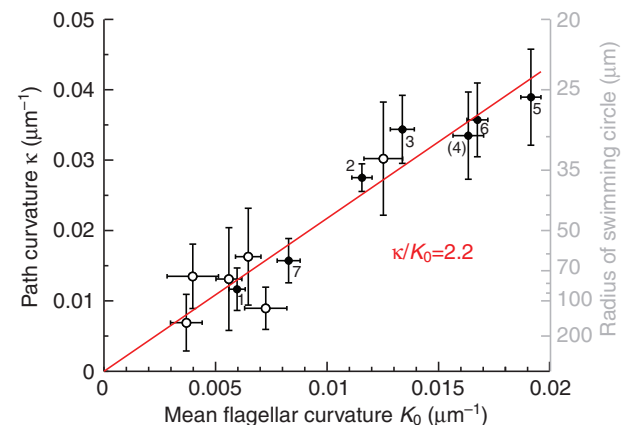

Fig. 5. A curved mean shape of the flagellum results in curved sperm swimming paths. Shown is path curvature κ *versus* mean flagellar curvature K_0 for 13 different bull sperm cells swimming close to a planar boundary surface. Experiments were performed either at normal viscosity $\eta \approx 0.7$ mPa s (solid circles, numbers correspond to Table 1) or at an increased viscosity $\eta \approx 10$ mPa s (open circles). Approximately, we find that path curvature κ scales linearly with mean flagellar curvature K_0 with a proportionality factor of about 2.2.

The linear dependence accords with theoretical predictions in the limit of small tangent angles (see Appendix). The fact that we find a factor of proportionality different from one reflects the non-linear character of flagellar self-propulsion at low Reynolds numbers: numerical simulations suggest that a ratio κ/K_0 significantly larger than one is a result of a finite amplitude of the flagellar beat as well as the presence of the hydrodynamic drag of the sperm head. Assuming a simplified beat pattern with tangent angle given by:

$$\psi(s,t) = K_0 s + 2A_0 s\cos(\omega t - 2\pi s/\lambda) , \qquad (8)$$

we numerically find an approximately linear dependence between mean flagellar curvature K_0 and path curvature κ provided the other parameters are held fixed (Fig. 6A). We find that the factor of proportionality between K_0 and κ depends on the amplitude parameter A_0 (see Fig. 6B). Increasing the friction coefficients of the sperm head also increased this factor. In the range of experimentally observed amplitude parameters $A_0 \approx 10–16\,\mathrm{rad\,mm^{-1}}$, we obtain proportionality factors in the range $d\kappa/dK_0 \approx 1.9–2.4$ consistent with the value $\kappa/K_0 \approx 2.2$ found by fitting experimental data. The proportionality factor is accounted for by the observed beat amplitude and thus eventually by the intrinsic non-linearity of the propulsion mechanism.

Flagellar curvature is an emergent property generated by active processes

We recorded planar flagellar beat patterns of bull sperm cells swimming at two different fluid viscosities, $\eta \approx 0.7\,\mathrm{mPa\,s}$ and $\eta \approx 10\,\mathrm{mPa\,s}$. Surprisingly, the mean flagellar curvature K_0 was reduced by a factor of two in the case of increased viscosity (see Table 2). This observation suggests that the mean shape of the flagellum is not solely determined by the asymmetric architecture of the passive flagellar components, which are not expected to change when the external viscosity is increased. Rather, the dependence of mean flagellar curvature on fluid viscosity suggests that flagellar asymmetry is an emergent property that depends on active processes within the flagellum.

DISCUSSION

In this paper, we used high-speed videoscopy and quantitative image analysis to obtain high-precision tracking data with sub-micrometre resolution for bull sperm cells swimming close to a planar boundary surface. From these tracking data, we computed the time series of instantaneous velocities of the sperm head which reveal insights into the fine structure of sperm swimming. The instantaneous velocities can be accurately reconstructed from the shape of the flagellar beat using resistive force theory. Furthermore, resistive force theory also accounts for the relationship between path curvature and mean flagellar curvature, which is characterized by a non-unitary factor of proportionality. Thus, this theory accounts for the swimming behaviour of sperm cells near a boundary surface, both at the sub-micrometre scale of wiggling head movements and also on a coarse-grained length scale on which sperm cells follow circular paths. The theory accounts for the non-linear nature of flagellar propulsion that is evident on all length scales. On the small scale, we observe, for example, a peculiar spectral feature of one of the instantaneous velocities (an enhanced second Fourier mode), which was predicted by our theoretical considerations. On the large scale, we accounted quantitatively for the relationship between path curvature and mean flagellar curvature.

Like the bull sperm cells studied here, sperm cells from many other species also swim along circular paths near surfaces (Rikmenspoel et al., 1960; Goldstein, 1977; Brokaw, 1979; Woolley, 2003; Kaupp et al., 2008; Riedel-Kruse et al., 2007), or even move along helical paths in three-dimensional space far from any boundary surface (Crenshaw, 1996; Corkidi et al., 2008). For sea urchin sperm cells, which have to find their eggs in open water, curved swimming paths are at the core of a chemotaxis mechanism that guides these sperm cells to the egg [see Kaupp et al. and Friedrich and Jülicher, and references therein (Kaupp et al., 2008; Friedrich and Jülicher, 2007)]. The observed curved swimming paths are a consequence of chiral propulsion by asymmetric flagellar bending waves. The asymmetry of the bending waves is in turn rooted in the chiral architecture of the sperm flagellum (Lindemann, 1994; Hilfinger and Jülicher, 2008), which possesses a defined handedness (Afzelius, 1999). Much progress has been made in recent years to theoretically explain the symmetric part of flagellar bending waves (Riedel-Kruse et al., 2007; Brokaw, 2008). However, why these planar flagellar waves are asymmetric is not fully understood. A steady-state activity of the molecular
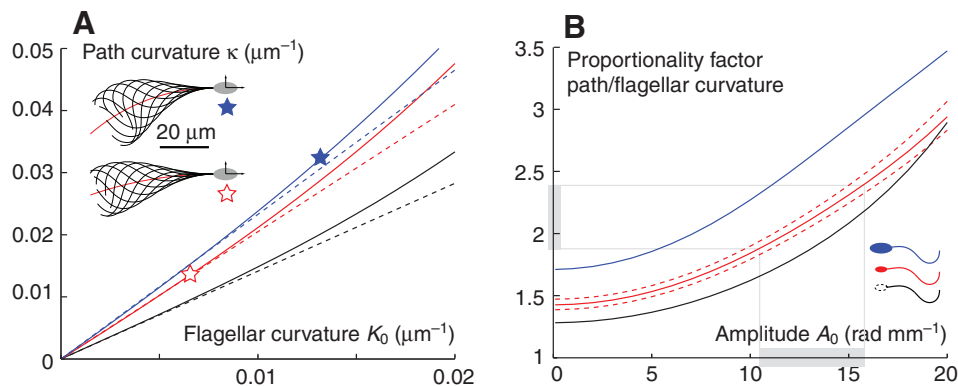

Fig. 6. (A) Dependence of path curvature κ on mean flagellar curvature K_0 for different values of the amplitude parameter A_0=0.1, 12.0, 14.6 rad mm^{-1} corresponding to the black, red and blue solid curve, respectively (numeric results assuming the simple flagellar beat pattern given in Eqn 8). Dashed lines correspond to a perturbation calculation valid to linear order in K_0. The inset shows example beat patterns corresponding to the data points marked by a symbol. (B) The factor of proportionality between mean flagellar curvature K_0 and path curvature κ depends on the amplitude A_0 of the flagellar beat (red curve). (The proportionality factor is computed as $d\kappa/dK_{0/K_0=0}$, which corresponds to the slope of the dashed curves in A.) For comparison, we also show the case of a headless sperm (black) and a case where the dimensions of the head have been doubled (blue). The grey region indicates the range of experimentally observed beat amplitudes. We used parameters in accordance with experimental data (see Table 1): $\xi_\perp/\xi_\parallel$=1.81 (unless otherwise stated), $\xi_\parallel$=0.69 fN s mm^{-2}, flagellar wavelength λ=L. The lower/upper dashed red curve corresponds to alternative values for the drag anisotropy ratio $\xi_\perp/\xi_\parallel$=1.81±0.07.

motors in the flagellum will generate pre-twist of the flagellum (Hilfinger and Jülicher, 2008), which may be at the origin of the observed asymmetry. Interestingly, we find here that the mean curvature of the flagellum depends on fluid viscosity. Additionally, previous work has shown that the intraflagellar calcium concentration is a key player in regulating the asymmetry of the flagellar beat (Brokaw, 1979; Cook et al., 1994; Böhmer et al., 2005; Wood et al., 2005). All these findings suggest that the mean curvature of the flagellum depends on active processes within the flagellum.

In this manuscript, we obtained the shape of the flagellar beat directly from the experiments and related these beat patterns quantitatively to the complex swimming paths of sperm cells. As such, our study contributes to explaining cell motility from basic swimming movements, which in turn are determined by the molecular architecture of the flagellar swimming apparatus.

APPENDIX
Flagellar propulsion in the limit of small tangent angles

For any periodic flagellar beat pattern with angular frequency ω, the instantaneous velocities $v_1(t)$, $v_2(t)$ and $\Omega(t)$ are periodic functions in time of period $T=2\pi/\omega$. We consider the most general beat pattern for which the tangent angle is characterized by its zeroth and first Fourier mode:

$$\psi(s,t) = \varepsilon_0 \tilde{\psi}_0(s) + \varepsilon_1 \tilde{\psi}_1(s)\exp(i\omega t) + cc \,, \quad (A1)$$

where cc denotes the complex conjugate. Here $\tilde{\psi}_0(s)$ and $\tilde{\psi}_1(s)$ are arbitrary functions of the arc length s, which describe the mean shape of the flagellum and the complex amplitude of the flagellar wave, repetively. The dimensionless scaling factors ε_0 and ε_1 allow adjustment of the mean flagellar curvature K_0 and the amplitude parameter A_0; they conveniently play the role of small parameters in the perturbation calculation given below. For the simple flagellar beat given by Eqn 8, we would have $\tilde{\psi}_0(s)=s/L$, $\tilde{\psi}_1(s)=s/L\exp(-2\pi i s/\lambda)$ as well as $\varepsilon_0=K_0 L$, $\varepsilon_1=A_0 L$. We can expand the instantaneous swimming velocities in the asymmetry factor ε_0 and the amplitude factor ε_1 as follows:

$$v_1(t) = \sum_{k,l,m} \varepsilon_0^k \varepsilon_1^l X_{k,l,m}(\psi_0,\psi_1)\exp(im\omega t) \,,$$

$$v_2(t) = \sum_{k,l,m} \varepsilon_0^k \varepsilon_1^l Y_{k,l,m}(\psi_0,\psi_1)\exp(im\omega t) \,,$$

$$\Omega_1(t) = \sum_{k,l,m} \varepsilon_0^k \varepsilon_1^l Z_{k,l,m}(\psi_0,\psi_1)\exp(im\omega t) \,. \quad (A2)$$

Under a reflection of the beat pattern, $\psi \rightarrow -\psi$, the velocity component $v_1(t)$ remains unchanged, whereas $v_2(t)$ and $\Omega(t)$ change their sign. Thus, all terms in the expansion for $v_1(t)$ for which $k+l$ is odd must vanish by symmetry; likewise, all terms in the expansions for $v_2(t)$ and $\Omega(t)$ with even $k+l$ are zero. Moreover, for any non-zero term in the expansions, the mode number $|m|$ is always smaller than the amplitude number l and has the same parity. Thus, to leading order, the above expansions read:

$$v_1(t) = \varepsilon_1^2 (X_{0,2,0} + X_{0,2,2} \exp 2i\omega t + cc) +$$
$$\varepsilon_0 \varepsilon_1 (X_{1,1,1} \exp i\omega t + cc) + O(\varepsilon_0^3 \varepsilon_1, \varepsilon_0^2 \varepsilon_1^2, \varepsilon_0 \varepsilon_1^3, \varepsilon_1^4) \,,$$

$$v_2(t) = \varepsilon_1 (Y_{0,1,1} \exp i\omega t + cc) + O(\varepsilon_0 \varepsilon_1^2, \varepsilon_1^3) \,,$$

$$\Omega(t) = \varepsilon_1 (Z_{0,1,1} \exp i\omega t + cc) + O(\varepsilon_0 \varepsilon_1^2, \varepsilon_1^3) \,. \quad (A3)$$

Averaging over one beat cycle, we find for the net speed of flagellar propulsion:

$$\bar{v} = \varepsilon_1^2 [X_{0,2,0} + 2 \,\mathrm{Im}\, Y_{0,1,1} Z_{0,1,1}^* / \omega] + O(\varepsilon_0^2 \varepsilon_1^2, \varepsilon_1^4) \,, \quad (A4)$$

The net rotational velocity is given by a higher order coefficient:

$$\bar{\Omega} = \varepsilon_0 \varepsilon_1^2 Z_{1,2,0} + O(\varepsilon_0 \varepsilon_1^4, \varepsilon_0^3 \varepsilon_1^2) \,. \quad (A5)$$

Note that the translational and rotational speed scale with the square of the beat amplitude ε_1^2, whereas the instantaneous speeds $v_2(t)$ and $\Omega(t)$ scale linearly with ε_1. This scaling behaviour is a hallmark of self-propulsion at low Reynolds numbers (Shapere and Wilczek, 1987; Lauga, 2007). Using force and torque balance Eqns 6 and 7, the coefficients $X_{k,l,m}$, $Y_{k,l,m}$ and $Z_{k,l,m}$ can be expressed as a linear combination of (products of) integrals involving $\tilde{\psi}_0$ and $\tilde{\psi}_1$. For the leading order coefficients, we find:

$$\begin{pmatrix} Y_{0,1,1} \\ Z_{0,1,1} \end{pmatrix} = i\omega \begin{pmatrix} \xi_2/\xi_\perp + L, & -L^2/2 \\ L^2/2, \xi_{\mathrm{rot}}/\xi_\perp - L^3/3 \end{pmatrix}^{-1} \cdot \begin{pmatrix} L^2[J_{0,1,1}^{(0)} - J_{0,1,1}^{(1)}] \\ L^3[J_{0,1,1}^{(1)} - J_{0,1,1}^{(2)}]/2 \end{pmatrix},$$

$$(\xi_1 + L\xi_\parallel)X_{0,2,0} = 2(\xi_\perp - \xi_\parallel)L\mathrm{Re}[i\omega L I_{0,2,0} + J_{0,1,1}^{(0)}Y_{0,1,1}^* - LJ_{0,1,1}^{(0)}Z_{0,1,1}] \,,$$
$$-2\xi_\parallel L^2 \mathrm{Re}[(J_{0,1,1}^{(0)} - J_{0,1,1}^{(1)})C_{0,1,1}^*] \,,$$

$$(\xi_1 + L\xi_\parallel)X_{1,1,1} = (\xi_\perp - \xi_\parallel)L[-i\omega L I_{1,1,1} + J_{1,0,0}^{(0)}Y_{0,1,1} - LJ_{1,0,0}^{(1)}Z_{0,1,1}]$$
$$-\xi_\parallel L^2[(J_{1,0,0}^{(0)} - J_{1,0,0}^{(1)})Z_{0,1,1} + i\omega J_{1,1,1}^{(0)} - J_{1,1,1}^{(1)})] \,, \quad (A6)$$

where we have introduced the dimensionless integrals:

$$J_{1,0,0}^{(k)} = \int_0^L \mathrm{d}s s^k \tilde{\psi}_0(s) / L^{k+1} \,,$$

$$J_{0,1,0}^{(k)} = \int_0^L \mathrm{d}s s^k \tilde{\psi}_1(s) / L^{k+1} \,,$$

$$J_{1,1,1}^{(k)} = \int_0^L \mathrm{d}s s^k \tilde{\psi}_0(s)\tilde{\psi}_1(s) / L^{k+1} \,,$$

$$I_{0,2,0} = \int_0^L \mathrm{d}s \tilde{\psi}_1(s) \int_0^s \mathrm{d}u \tilde{\psi}_1^*(u) / L^2,$$

$$I_{1,1,1} = \int_0^L \mathrm{d}s \tilde{\psi}_0(s) \int_0^s \mathrm{d}u \tilde{\psi}_1(u) / L^2,$$

For the sake of illustration, we study as an example the simple flagellar beat pattern whose tangent angle is given by Eqn 8. For simplicity, we neglect the hydrodynamic drag force of the sperm head, i.e. $\xi_1=\xi_2=0$, $\xi_{\mathrm{rot}}=0$. We also assume that the wave number n is an integer. Then the coefficients relevant for the net translational and rotational speed, $\bar{v}$ and $\bar{\Omega}$, respectively, are given by:

$$X_{0,2,0} = \Theta_v \left(\frac{\xi_\perp}{\xi_\parallel} - 1\right) \frac{L}{nT} - 2\,\mathrm{Im}\, Y_{0,1,1}Z_{0,1,1}^* / \omega$$

$$Z_{1,2,0} = \left[\Theta_\Omega^{(0)} + \Theta_\Omega^{(1)}\frac{\xi_\perp}{\xi_\parallel} + \Theta_\Omega^{(-1)}\frac{\xi_\parallel}{\xi_\perp}\right]\frac{1}{nT} \,, \quad (A7)$$

and $Y_{0,1,1}=2\omega L^2(9+i\pi n)/(2\pi n)^3$, $Z_{0,1,1}=12\omega L(3+i\pi n)/(2\pi n)^3$, $X_{1,1,1}=0$. The prefactors Θ_v, $\Theta_\Omega^{(k)}$ depend on the wave number n and read $\Theta_v=(2/3)-2\mu-9\mu^2$, $\Theta_\Omega^{(0)}=(3/5)-(9/2)\mu^2-216\mu^3$, $\Theta_\Omega^{(1)}=-(2/3)+2\mu+9\mu^2$, $\Theta_\Omega^{(-1)}=(1/15)-6\mu+(3/2)\mu^2+432\mu^3$, where we have used the short-hand notation $\mu=1/(\pi n)^2$.

We remark on some properties of the Eqns A4, A5 and A7 for the net velocities $\bar{v}$ and $\bar{\Omega}$: the direction of forward propulsion is opposite to the propagation direction of the flagellar travelling wave, provided $\xi_\perp > \xi_\parallel$ (Brennen and Winet, 1977). In the case of isotropic drag coefficients $\xi_\parallel = \xi_\perp$, the translational speed $\bar{v}$ vanishes [see Becker et al. for a general proof of this fact (Becker et al., 2003)]. The sperm cell will swim along a circular swimming path with a curvature $\kappa=\bar{\Omega}/\bar{v}$

that is proportional to the curvature K_0 of the mean shape of the flagellum. A similar result was found by Keller and Rubinow (Keller and Rubinow, 1976). Even for a symmetric beat pattern with $K_0=0$, the instantaneous rotational speed $\Omega(t)$ oscillates with the frequency ω of the flagellar beat. Of course, the averaged rotational speed $\bar{\Omega}$ vanishes in this case, $\bar{\Omega}=0$, as is required by symmetry. The case of a symmetric flagellar beat with $K_0=0$ was first addressed by Taylor, and Gray and Hancock (Taylor, 1952; Gray and Hancock, 1955) and re-examined by Shack and colleagues (Shack et al., 1974). Note that Taylor, and Gray and Hancock (implicitly) imposed the constraint $\Omega(t)=0$ for their calculation (Taylor, 1952; Gray and Hancock, 1955). With this constraint, the expressions for the translational speeds $v_j(t)$ look different. If we had imposed the constraint $\Omega(t)=0$ in our calculation, we would find a different prefactor $\Theta_v=(2/3)-\mu/2$ for the net translational speed. These differences in the expression for $\bar{v}$ highlight the role of constraints in microswimming problems.

LIST OF SYMBOLS AND ABBREVIATIONS

Shape of the flagellar beat

A_0	amplitude parameter of flagellar bending wave – defined as slope of $\tilde{\psi}_1(s)$
K_0	mean flagellar curvature – defined as slope of $\tilde{\psi}_0(s)$
$\mathbf{r}(s,t)$	centreline of sperm flagellum as function of arc length s and time t
λ	wavelength of (principal) flagellar bending wave
$\psi(s,t)$	tangent angle characterizing flagellar shape
$\tilde{\psi}_0(s)$	zeroth Fourier mode of ψ (characterizing time-averaged shape of flagellum)
$\tilde{\psi}_1(s)$	first Fourier mode of ψ (characterizing symmetric part of flagellar waves)
ω, $T=2\pi/\omega$	angular frequency and period of the flagellar beat

Dynamics of sperm swimming

$\mathbf{e}_1(t)$, $\mathbf{e}_2(t)$	unit vectors parallel and perpendicular to the long axis of the sperm head
$\mathbf{r}(t)$	position of the center of the sperm head as function of time t
$\bar{\mathbf{r}}(t)$	coarse-grained sperm swimming path that averages over sub-cycle motion
$v_1(t)$, $v_2(t)$	instantaneous speed of sperm head for motion in the direction $\mathbf{e}_1$, $\mathbf{e}_2$, respectively
$\bar{v}$, $\bar{\Omega}$	net translational and angular speed along the path $\bar{\mathbf{r}}$
κ	curvature of coarse-grained swimming path $\bar{\mathbf{r}}$
$\Omega(t)$	instantaneous angular speed of the sperm head (in the plane of swimming)

Hydrodynamic drag

$\mathbf{f}(s,t)$	hydrodynamic drag force density along the flagellar length
$\xi_\parallel$, $\xi_\perp$	effective hydrodynamic drag coefficients of the sperm flagellum for motion parallel and perpendicular to its centreline, respectively

REFERENCES

Afzelius, B. A. (1999). Asymmetry of cilia and flagella of mice and men. *Int. J. Dev. Biol.* **43**, 2283-2286.

Becker, L. E., Koehler, S. A. and Stone, H. A. (2003). On self-propulsion of micromachines at low Reynolds number: Purchell's three-link swimmer. *J. Fluid Mech.* **490**, 15-35.

Böhmer, M., Van, Q., Weyand, I., Hagen, V., Beyermann, M., Matsumoto, M., Hoshi, M., Hildebrand, E. and Kaupp, U. B. (2005). Ca²⁺-spikes in the flagellum control chemotactic behaviour of sperm. *EMBO J.* **24**, 2741-2752.

Brennen, C. and Winet, H. (1977). Fluid mechanics of propulsion by cilia and flagella. *Ann. Rev. Fluid Mech.* **9**, 339-398.

Brokaw, C. J. (1966). Effects of increased viscosity on the movements of some invertebrate spermatozoa. *J. Exp. Biol.* **45**, 113-139.

Brokaw, C. J. (1970). Bending moments in free-swimming flagella. *J. Exp. Biol.* **53**, 445-464.

Brokaw, C. J. (1979). Calcium-induced asymmetrical beating of triton-demembranated sea urchin sperm flagella. *J. Cell Biol.* **82**, 401-411.

Brokaw, C. J. (2008). Thinking about flagellar oscillation. *Cell Motil. Cytoskel.* **66**, 425-436.

Cook, S. P., Brokaw, C. J., Muller, C. H. and Babcock, D. F. (1994). Sperm chemotaxis: Egg peptides control cytosolic calcium to regulate flagellar responses. *Dev. Biol.* **165**, 10-19.

Corkidi, G., Taboada, B., Wood, C. D., Guerrero, A. and Darszon, A. (2008). Tracking sperm in three-dimensions. *Biochem. Biophys. Res. Comm.* **373**, 125-129.

Cox, R. G. (1970). The motion of long slender bodies in a viscous fluid. Part 1. General theory. *J. Fluid Mech.* **44**, 791-810.

Crenshaw, H. C. (1996). A new look at locomotion in microorganisms: Rotating and translating. *Americ. Zool.* **36**, 608-618.

Dresdner, R. D. and Katz, D. F. (1981). Relationships of mammalian sperm motility and morphology to hydrodynamic aspects of cell function. *Biol. of Reprod.* **25**, 920-930.

Elgeti, J. and Gompper, G. (2008). Hydrodynamics of active mesoscopic systems. In *NIC Symposium 2008*, Vol. 39 (ed. G. Münster, D. Wolf and M. Kremer), pp. 53-62. Jülich: John von Neumann Institute for Computing.

Friedrich, B. M. and Jülicher, F. (2007). Chemotaxis of sperm cells. *Proc. Natl. Acad. Sci. USA* **104**, 13256-13261.

Goldstein, S. F. (1977). Asymmetric waveforms in echinoderm sperm flagella. *J. Exp. Biol.* **71**, 157-170.

Gray, J. (1955). The movement of sea-urchin spermatozoa. *J. Exp. Biol.* **32**, 775-801.

Gray, J. and Hancock, G. T. (1955). The propulsion of sea-urchin spermatozoa. *J. Exp. Biol.* **32**, 802-814.

Hilfinger, A. and Jülicher, F. (2008). The chirality of ciliary beats. *Phys. Biol.* **5**, 1-12.

Hunt, A. J., Gittes, F. and Howard, J. (1994). The force exerted by a single kinesin molecule against a viscous load. *Biophys. J.* **67**, 766-781.

Johnson, R. E. and Brokaw, C. J. (1979). Flagellar hydrodynamics. *Biophys. J.* **25**, 113-127.

Jülicher, F. and Prost, J. (2009). Generic theory of colloidal transport. *Eur. Phys. J. E* **29**, 27-36.

Kaupp, U. B., Kashikar, N. D. and Weyand, I. (2008). Mechanisms of sperm chemotaxis. *Annu. Rev. Physiol.* **70**, 93-117.

Keller, J. B. and Rubinow, S. I. (1976). Swimming of flagellated microorganisms. *Biophys. J.* **16**, 151-170.

Landau, L. D. and Lifshitz, E. M. (1987). *Fluid Mechanics*. New York: Butterworth-Heinemann.

Lauga, E. (2007). Floppy swimming: viscous locomotion of actuated elastica. *Phys. Rev. E* **75**, 041916.

Lighthill, J. L. (1976). Flagellar hydrodynamics. *SIAM Rev.* **18**, 161-230.

Lindemann, C. B. (1994). A 'geometric clutch' hypothesis to explain oscillations of the axoneme of cilia and flagella. *J. Theoret. Biol.* **168**, 175-189.

Miller, R. L. (1985). Sperm chemo-orientation in the metazoa. In *Biology of Fertilization. Biology of the Sperm*, Vol. 2 (ed. C. B. Metz and A. Monroy), pp. 275-337. New York: Academic Press.

Perrin, F. (1934). Mouvement Brownien d'un ellipsoide (l). Dispersion dièlectrique pour des molécules ellipsoidales. *J. Phys. Radium* **7**, 497-511.

Purcell, E. M. (1977). Life at low Reynolds numbers. *Am. J. Phys.* **45**, 3-11.

Riedel-Kruse, I. H., Hilfinger, A., Howard, J. and Jülicher, F. (2007). How molecular motors shape the flagellar beat. *HFSP* **1**, 192-208.

Rikmenspoel, R. (1965). The tail movement of bull spermatozoa. Observations and model calculations. *Biophys. J.* **5**, 365-392.

Rikmenspoel, R., van Herpen, G. and Eijkhout, P. (1960). Cinematographic observations of the movements of bull sperm cells. *Phys. Med. Biol.* **5**, 167-181.

Rothschild (1963). Non-random distribution of bull spermatozoa in a drop of sperm suspension. *Nature* **198**, 1221-1222.

Shack, W. J., Fray, C. S. and Lardner, T. J. (1974). Observations on the hydrodynamics and swimming motions of mammalian spermatozoa. *Bull. Math. Biol.* **36**, 555-565.

Shapere, A. and Wilczek, F. (1987). Self-propulsion at low Reynolds number. *Phys. Rev. Lett.* **58**, 2051-2054.

Smith, D. J., Gaffney, E. A., Blake, J. R. and Kirkman-Brown, J. C. (2009). Human sperm accumulation near surfaces: a simulation study. *J. Fluid Mech.* **621**, 289-320.

Taylor, G. I. (1951). Analysis of the swimming of microscopic organisms. *Proc. R Soc. Lond. A* **209**, 447-461.

Taylor, G. I. (1952). The action of waving cylindrical tails in propelling microscopic organisms. *Proc. R Soc. Lond. A* **211**, 225-239.

Winet, H., Bernstein, G. S. and Head, J. (1984). Observations on the response of human spermatozoa to gravity, boundaries and fluid shear. *J. Reprod. Fert.* **70**, 511-523.

Wood, C. D., Nishigaki, T., Furuta, T., Baba, A. S. and Darszon, A. (2005). Real-time analysis of the role of Ca²⁺ in flagellar movement and motility in single sea urchin sperm. *J. Cell Biol.* **169**, 725-731.

Woolley, D. M. (2003). Motility of spermatozoa at surfaces. *Reprod.* **126**, 259-270.

Yundt, A. P., Shack, W. J. and Lardner, T. J. (1975). Applicability of hydrodynamic analyses of spermatozoan motion. *J. Exp. Biol.* **62**, 27-41.